The effects of anion and cation substitution on the ultrafast solvent dynamics of ionic liquids: A time-resolved optical Kerr-effect spectroscopic study

Gerard Giraud
Department of Physics, University of Strathclyde, Glasgow G4 0NG, Scotland, United Kingdom

Charles M. Gordon and Ian R. Dunkin
Department of Pure and Applied Chemistry, University of Strathclyde, Glasgow G1 1XL, United Kingdom

Klaas Wynne[a)]
Department of Physics, University of Strathclyde, Glasgow G4 0NG, Scotland, United Kingdom

(Received 30 January 2003; accepted 4 April 2003)

Ultrafast solvent dynamics of room-temperature ionic liquids have been investigated by optical heterodyne-detected Raman-induced Kerr-effect spectroscopy (OHD-RIKES) by studying the effects of cation and anion substitution on the low frequency librational modes. The spectra of two series of imidazolium salts are presented. The first series is based on the 1-butyl-3-methylimidazolium salts $[\mathrm{bmim}]^+$ containing the anions trifluoromethanesulfate $[\mathrm{TfO}]^-$, *bis*(trifluoromethanesulfonyl)imide $[\mathrm{Tf_2N}]^-$, and hexafluorophosphate $[\mathrm{PF_6}]^-$. The second series is based on $[\mathrm{Tf_2N}]^-$ salts containing the three cations 1-butyl-2,3-dimethylimidazolium $[\mathrm{bmmim}]^+$, 1-methyl-3-octylimidazolium $[\mathrm{omim}]^+$, and $[\mathrm{bmim}]^+$. It is found in all five samples that the signal is due to libration of the imidazolium ring at three frequencies around 30, 65, and 100 cm^{-1} corresponding to three local configurations of the anion with respect to the cation. © *2003 American Institute of Physics.* [DOI: 10.1063/1.1578056]

I. INTRODUCTION

Room-temperature ionic liquids consist of organic cations combined with a wide range of inorganic or organic anions. This particular structure makes them nonvolatile, nonflammable, and polar. These properties have prompted a flurry of research on the possibility of using ionic liquids for clean chemical synthesis and catalysis.[1] However, relatively little is known about the microscopic physical properties of ionic liquids and how to predict the influence of these solvents on chemical reactions rates. Such understanding would improve the design and enhance the tunability of ionic liquids.

In very general terms, the role of the solvent in promoting a chemical reaction is to alter the energies of the reactant and product states in order to optimize the probability of jumping from one electronic state to another.[2] In a purely static view, this implies a rearrangement of charges in the solvent described by the dielectric constant in response to an altered charge distribution on the solute. From a dynamic point of view, states with different charge distributions are solvated on a femtosecond to picosecond timescale by solvent modes. Solvent modes range from diffusive reorientational motion (on a 1 to 200-ps time scale), through intermolecular librational motions (on a 100-fs to 1-ps time scale), to intramolecular vibrational motions (on a sub-100-fs time scale). However, a typical chemical reaction takes place on a timescale of about a picosecond and therefore only solvent motions occurring on a similar timescale (corresponding to the frequency range 0–200 cm^{-1}) will influence the reaction. On a longer time scale, the relaxation of the product state to equilibrium causes energy exchange with the medium that may also involve higher frequency modes.

The low-frequency dielectric response of ionic liquids can be accessed directly via far-infrared or terahertz (THz) absorption spectroscopy.[3] However, the study of ionic liquids by THz spectroscopy is currently limited by the phonon-band absorption of the semiconductors used to generate THz radiation, which make them opaque at frequencies between 100 and 200 cm^{-1}.[4] A possible alternative to THz spectroscopy is optical heterodyne-detected Raman-induced Kerr-effect spectroscopy (OHD-RIKES).[5,6] This technique has proven to be far superior to Raman spectroscopy at low frequencies (<400 cm^{-1}), and its high signal to noise ratio allows a detailed analysis of the spectra of liquids[5,7,8] and even solutions of organic molecules[9] and peptides.[10] This polarization-spectroscopy technique provides a signal linear in the third-order nonlinear optical response of the sample. Information is obtained regarding ultrafast solvent dynamics by measuring the time response of a transient birefringence that is induced in the sample by a polarized femtosecond optical pulse. On a long time scale (several picoseconds or more), the polarization-anisotropy decay is caused by the rotational diffusion of individual molecules[11] or ion-pairs[12] and reflects the general diffusive nature of relaxation on this time scale. On a shorter time scale (several hundreds of femtoseconds), the liquid dynamics is nondiffusive and instead inertial.[13] The inertial motions are governed by intermolecu-

a)Tel: +44 (141) 548 3381; Fax: +44 (141) 552-2891; Electronic mail: klaas.wynne@phys.strath.ac.uk

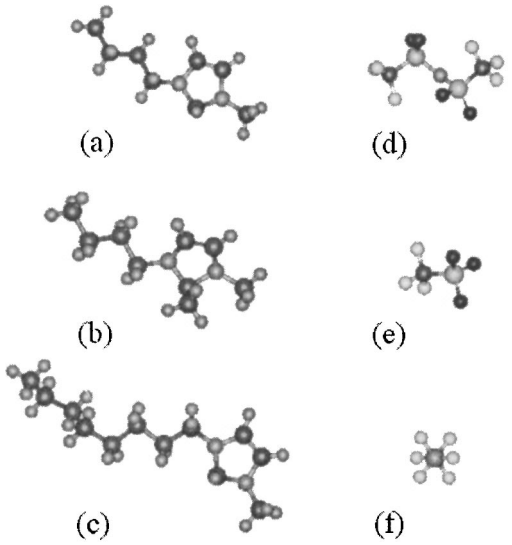

FIG. 1. Structure of anions and cations constituting the room-temperature ionic liquids studied here. (a) $[bmim]^+$ ($C_8H_{15}N_2$); (b) $[bmmim]^+$ ($C_9H_{17}N_2$); (c) $[omim]^+$ ($C_{12}H_{23}N_2$); (d) $[Tf_2N]^-$ ($[(CF_3SO_2)_2N]^-$); (e) $[TfO]^-$ $[(CF_3SO_3)]$; (f) $[PF_6]^-$.

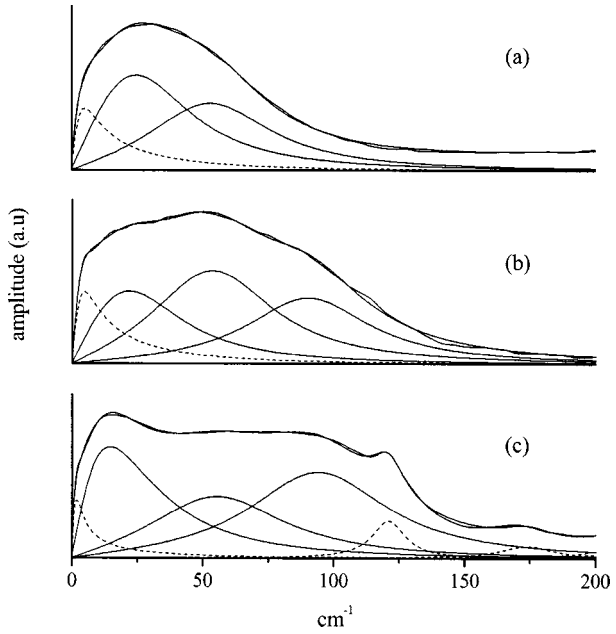

FIG. 2. Imaginary part of the Fourier transform of the ultrafast optical heterodyne-detected Raman-induced Kerr-effect spectroscopy (OHD-RIKES) signal normalized with the Fourier transform of the laser-pulse autocorrelation for (a) cyclohexane, (b) DMSO, and (c) $[bmim][Tf_2N]$. The spectra have been fitted with a Brownian oscillator model as described in the text. The dashed curve at very low frequency (<50 cm^{-1}) accounts for a residual rotational diffusion component, the solid lines represent librational motions, and the dashed lines at higher frequency (>100 cm^{-1}) represent intramolecular modes.

lar librational, translational, and collision-induced dynamics. On the shortest timescales, a sharp instantaneous peak is observed characteristic of the off-resonance electronic hyperpolarizability. Infrared-absorption spectroscopy is proportional to the first derivative of the dipole moment with respect to the relevant molecular coordinate[6,14] and is directly proportional to the dielectric function. The OHD-RIKES signal is proportional to the polarizability derivative.[6] Therefore, in principle, the amplitudes in the OHD-RIKES spectrum cannot be related in a simple way to those in the infrared spectrum. However, it has been shown[6] that in practice the Raman spectrum can be related to the infrared spectrum with reasonable accuracy.

Below we will present measurements of the ultrafast OHD-RIKES transients and spectra of a series of five prototypical room-temperature ionic liquids[15] (see Fig. 1): $[bmmim][Tf_2N]$, $[bmim][PF_6]$, $[bmim][Tf_2N]$, [bmim][TfO], and $[omim][Tf_2N]$. This particular set of five liquids allows the study of the effect of both subtle modification (cation-type) and gross modification (anion-type) on the low frequency spectra of those liquids. Increasing the length of *N*-alkyl substituents at the imidazolium ring of the cation results in an increase in the viscosity of the liquid at any particular temperature, as well as generally increasing the hydrophobic nature of the salt. The introduction of a methyl group at the 2-position on the ring results in a considerable decrease in the polarity of the ionic liquid. Different anions can also give room-temperature ionic liquids of distinctly different character with regard to properties such as viscosity and miscibility with other solvents. For example, considering the $[bmim]^+$ salts under investigation here, [bmim][TfO] is completely miscible with water, while the equivalent $[Tf_2N]^-$ and $[PF_6]^-$ salts are water immiscible. The order of viscosity of the salts in this series is $[bmim][TfO] < [bmim][Tf_2N] \ll [bmim][PF_6]$. Thus, these materials may be regarded as ''designer solvents,'' whose behavior may be tuned to particular applications depending on their structure.[1,16]

The analysis of the OHD-RIKES data was carried out in the frequency domain using fast Fourier-transformation and nonlinear least-squares fitting techniques. The OHD-RIKES spectra were fitted with a number of Brownian oscillators[17] to reproduce the broad intermolecular low frequency band. Although the Brownian-oscillator model gives slightly worse fits[5,17] than the more common models,[13,18] it also provides more insight into the underlying physics driving the low frequency dynamic in the liquid. The curves presented in Fig. 2 show the OHD-RIKES spectra for three simple liquids: cyclohexane, dimethylsulfoxide (DMSO), and $[bmim][Tf_2N]$. The spectra have been ordered from top to bottom by increasing viscosity and increasing polarity of the respective liquids. These three OHD-RIKES spectra are representative in that they display a common trend. It can be seen that an increase of the strength of the intermolecular interaction is accompanied by an increase in complexity of the low-frequency spectrum. Cyclohexane is nonpolar and displays a ''single'' broad shoulder. DMSO has a permanent dipole moment implying stronger interaction between solvent molecules. Hence, the DMSO low frequency band is broader and more structured than the corresponding band in the cyclohexane spectrum. Ionic liquids consist of dissociated ions in solution and hence experience strong coulombic interactions in addition to hydrogen bonds. This is reflected by very localized peaks in the low-frequency spectrum of $[bmim][Tf_2N]$ reflecting the strength of those interactions. Below, the specifics of those interactions will be discussed by con-

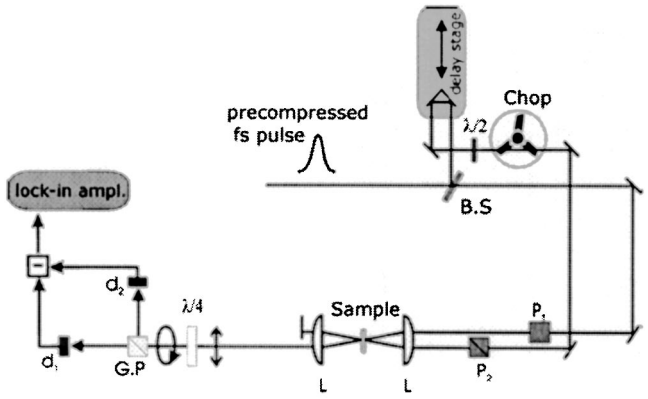

FIG. 3. Schematic diagram of the experimental OHD-RIKES setup used to perform the experiments described here. P_1 and P_2 represent polarizers, BS a beamsplitter, Chop a 1-kHz light chopper, and L a pair of lenses. λ/2 is a zero-order half-wave retardation plate, λ/4 a quarter-wave retardation plate, GP a Glan–Thompson polarizer, and d_1 and d_2 photodiodes wired up for balanced detection.

structing a detailed analysis of the intermolecular motions occurring in the five ionic liquids studied.

The paper is organized as follows: In the Experiment, the method of collecting the OHD-RIKES data in the time domain will be explained and in particular, the balanced detection technique we have used. In the Data Analysis, the procedure for cleaning up the time-domain data, the deconvolution, and Fourier-transformation procedure, and the nonlinear least-squares fitting procedures will be described in detail. The General Theory presents a simple classical model for predicting the strength of low-frequency librational Raman bands. This simple theory is of great value in understanding the experimental OHD-RIKES spectra obtained for the room-temperature ionic liquids. The section on Experimental Results and Discussion presents the experimental data and an analysis in terms of the structure of the liquid.

II. EXPERIMENT

The synthesis and purification of the ionic liquids studied here were performed as described previously.[16,19] It is known that the presence of even small quantities of water can result in considerable changes in the physical properties of ionic liquids,[20] and also that even water-immiscible ionic liquids can absorb considerable amounts of water. Therefore, all samples were dried by heating at 70 °C under vacuum for several hours and transferred to a 1-mm path length sealed glass cell for the spectroscopic experiments.

The ultrafast OHD-RIKES measurements (see Fig. 3) were carried out using linearly polarized laser pulses with a center wavelength of 800 nm, a 19-fs pulse duration (sech^2), and with good long-term stability. The pulses were generated in a homebuilt Kerr-lens mode-locked Ti:sapphire laser[21] pumped by a 5 W (CW) intracavity-doubled diode-pumped Nd:YAG laser (Coherent Verdi). To compensate for the positive dispersion induced by the optics in the setup, the beam was negatively chirped (or precompensated) with a pair of prisms placed after the oscillator. The laser beam was split into a pump beam (~80%) and a probe beam (~20%) by a beamsplitter, and the pump beam was optically delayed using a 50-nm resolution stepper motor. Polarizers were placed in both arms to achieve a 45° angle between pump and probe-beam polarization. A 6-cm focal-length lens was used to focus the two beams into the sample. Phase-sensitive detection was achieved with a 1-kHz chopper in the pump beam and lock-in amplification. The pulse width was measured at the sample position as 19 fs FWHM by two-photon absorption in a GaP PIN photodiode.[22]

The ultrafast birefringence signal was obtained with a shot-noise limited balanced-detection system unlike the method used in a traditional OHD-RIKES setup.[23] In a traditional setup, a quarter-wave retardation plate is positioned between two crossed polarizers in the probe beam and oriented with its ''fast'' axis parallel to the polarization plane of the probe beam. The transmission of the Kerr cell is detected with a single photodiode/lock-in-amplifier combination. In this particular case, the signal recorded is the homodyne signal, which is proportional to the square of the nonlinear susceptibility of the sample. By rotating the input polarizer slightly (≈1°), a small orthogonal polarization component is introduced. This so-called local oscillator introduces a heterodyne component to the signal (linear in the nonlinear susceptibility of the sample) on top of a constant background (from the laser). Therefore, three terms appear in the expression of the signal intensity: a constant background, a homodyne signal, and a heterodyne signal. The constant background is electronically subtracted. To eliminate the homodyne ''contamination'' of the signal, two sets of data must be collected with positively and negatively sensed local oscillators. However, heterodyne OHD-RIKES data collection can be both simplified and enhanced using balanced detection. In our setup, the probe beam is fully circularly polarized with a quarter-wave retardation plate after the sample. Parallel and perpendicular components are separated with a Glan–Thompson polarizer and sent to a pair of photodiodes wired up for balanced detection.[24] Because the signal is obtained by *electronically* subtracting the horizontal from the vertical component, both homodyne and background components cancel. In turn, the pure heterodyne signal is recorded in a single shot. In addition, balanced detection reduces the effects of random fluctuations of the laser power and achieves a significant improvement in the signal to noise ratio. Furthermore, by balancing with either a quarter or a half-wave retardation plate, either a signal purely due to birefringence or purely due to dichroism is measured as can be shown with a Jones-matrix analysis of the optical setup (see Appendix).

III. DATA ANALYSIS

Data analysis can be performed either in the time or in the frequency domain. Relaxation processes are more easily visualized in the time domain but for analyzing the intermolecular dynamics, it is easier and more meaningful to work in the frequency domain. Because experimental spectra can be fitted to a large number of line-shape combinations, a proper error analysis is crucial but not typically done by others. The first part of this section explains how the data are sampled and transformed to the frequency domain; the second part concentrates on the actual analysis of the spectrum.

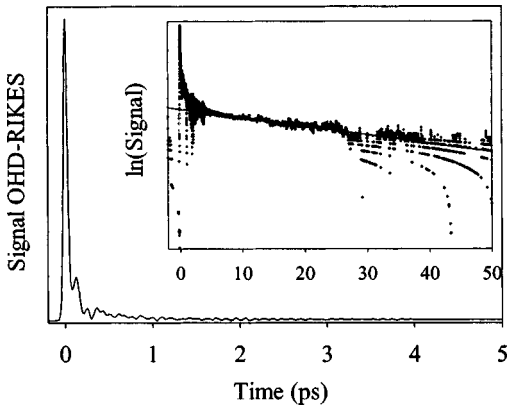

FIG. 4. Unprocessed OHD-RIKES time-domain data of [bmmim][Tf_2N]. The inset shows the logarithm of the same signal. The data are fitted on a logarithmic scale from 6 to 30 ps to a straight line corresponding to a single exponential decay. This exponential decay is subsequently subtracted from the time-domain data prior to Fourier transformation to the frequency domain.

A. Time to frequency domain

The OHD-RIKES signal is measured in the time domain and therefore any analysis has to start there. Because ultrashort pulses are not instantaneous, the observed signal $S(t)$ in the ultrafast OHD-RIKES experiment is the convolution of the second-order autocorrelation function of the laser pulse $G_2(t)$ with the molecular nonlinear response $R(t)$,[23]

$$S(t) \propto \int_{-\infty}^{t} d\tau R(t-\tau) G_2(\tau). \tag{1}$$

The impulse response function is obtained by deconvolution of the experimental signal yielding $R(\omega)$.[25] It can be shown that because of the symmetry properties of the nonlinear response in the time domain, the imaginary part of $R(\omega)$ is purely related to the nuclear part of the transient birefringence.[26] The resulting spectrum is equal to the low-frequency depolarized Rayleigh spectrum multiplied by a Bose thermal-occupation factor,[17]

$$\mathrm{Im}\, R_{\text{OHD-RIKES}}(\omega) = R_{\text{DRS}}(\omega)[1-\exp(-\hbar\omega/k_B T)]. \tag{2}$$

In our experiments, data were recorded from -1 ps to 70 ps. An example of the signal in the time domain is given in Fig. 4 for [bmim][Tf_2N]. A sharp peak corresponding to the electronic response of the sample arises at time zero, followed by the librational ultrafast dynamics in the first picosecond, and a subsequent slow exponential tail attributed to rotational diffusion. Before transformation to the frequency domain, a careful manipulation of the raw time-domain data is required in order to maximize the signal to noise ratio as well as the physical accuracy of the spectrum. Because the spectrum is obtained by Fourier transformation of the OHD-RIKES time-domain signal, any noise present in the long-time tail of the signal (due to dramatic decrease of the signal strength at long delays) is observed in the low frequency part of the spectrum. This can be avoided by fitting the slow rotational-diffusion component of the signal with a single exponential decay from 6 ps to the end of the data set. A new data file is created made of the experimental points from -2 to 6 ps and the fitted tail from 6 ps to the end of the data at 30 ps.

A valid spectrum is only obtained if the time reference (zero delay between pump and probe beam) of the autocorrelation and birefringence signals is identical. Because the autocorrelation and birefringence signals have to be measured separately, their respective zero delay position is slightly shifted, if only by a few femtoseconds typically. It is therefore necessary to match the reference time of the two signals. This was done empirically by correcting the zero delay of the signal (typically by $+6$ to $+10$ fs) in order to obtain a spectrum that is positive from 0 cm^{-1} to the highest possible frequency while at the same time minimizing any background. Finally, in order to characterize the spectral features that correspond to the inertial dynamics in the frequency domain, the long-time rotational-diffusion component is subtracted from the raw time-domain data.

Once the spectrum has been obtained by deconvolution, a final point must be taken into account prior to the lineshape analysis. The amplitude of an experimental OHD-RIKES spectrum is arbitrary, notably because of power fluctuations of the laser or misalignment of the setup due to temperature fluctuations. In order to compare the relative amplitudes of the different spectra, it is necessary to normalize the signal. Because all five samples consist of a similar cation with an imidazolium ring, their electronic hyperpolarizability can be assumed to be identical. The electronic response of the sample appears as a constant background in the *real* part of the deconvoluted OHD-RIKES spectrum. Therefore, the spectra presented here were normalized using this electronic response.

B. The fitting procedure

All OHD-RIKES spectra present some general features: a sharp peak at very low frequency corresponding to a diffusional reorientational response, narrow bands at frequencies greater than $\sim$200 cm^{-1} associated with intramolecular modes, and broad low-frequency bands typically below 200 cm^{-1} reflecting the intermolecular librational motions in the liquid. Apart from the main rotational-diffusion component that has been subtracted in the time domain (see above), those features can be observed in Figs. 2, 7, and 10. The three main spectral regions are discussed in more detail below.

According to previous work,[12] ionic liquids with an organic chain containing two to eight carbon atoms have an orientational-diffusion time greater than 200 ps. In our set of five samples, two rotational-diffusion components have been observed. Because the time-domain OHD-RIKES signal decays by about two orders of magnitude in only a few picoseconds, the slow relaxation decay was simply subtracted from the time-domain data with no attempt to discuss their relative decay-rate values. The fast relaxation decay was fitted in the frequency domain to an overdamped Lorentzian function [Eq. (5)] as shown by the dashed curve in Fig. 5. In our fits, the overdamped Lorentzian corresponds to relaxation on a time scale from 1 to 3 ps with no obvious relation to the particular ionic structure. Recent studies of dielectric

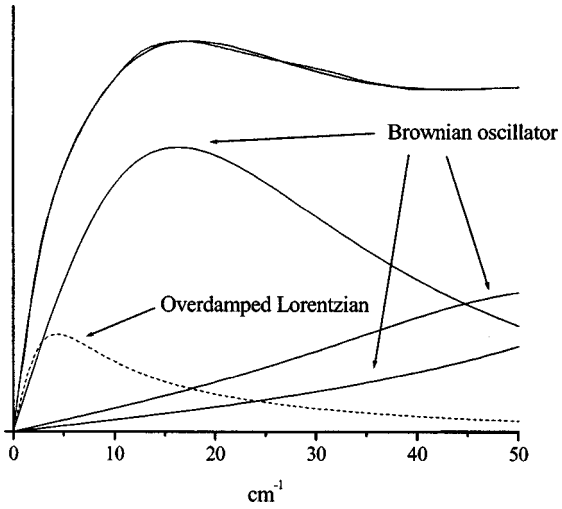

FIG. 5. Close up of the first 50 cm^{-1} of the experimental OHD-RIKES spectrum of [bmmim][Tf_2N] and the individual components of the nonlinear least-squares fit to the data.

relaxation of molten salts[11] have revealed a ''main'' relaxation component ($\tau_1 = 2.6$ ps) associated with correlated bulk motion in the salt, a fast ''second'' relaxation component ($\tau_2 = 0.24$ ps) assigned to hydrogen-bond dynamics, and an unresolved ''ultrafast'' relaxation ($\tau_3 < 30$ fs).

The high frequency bands ($> \approx 200$ cm^{-1}) correspond to intramolecular vibrations. Unlike the broad low frequency bands they are represented by well separated and often narrow features in the spectrum. From a fitting point of view, they are characterized by single Lorentzians.

As mentioned in the Introduction, the low frequency intermolecular librations are crucial in determining chemical-reaction rates. The dipole moment involved in the libration can be either permanent or induced. In the latter case, this may result from a field through the molecule's polarizability or by collisional interactions. The relative strength of these components in the signal strongly depends on the nature of the sample. For highly polarizable and anisotropic molecules, collision-induced interactions can be all but disregarded. However, in the case of spherical molecules, the molecular polarizability does not depend on the molecular orientation and the signal depends on interaction-induced effects.

The coupling between the atomic-displacement coordinates of a mode and the static and dynamic forces in the surrounding medium leads to the broadening of a vibrational band. OHD-RIKES spectroscopy cannot distinguish between quasistatic ''inhomogeneous'' and fast ''homogeneous'' contributions to the distribution of frequencies. That distinction can only be made in principle with higher order Raman techniques such as six-wave mixing[27] or Raman photon echoes.[28] However, the interpretation of the experimental signal from such higher order Raman techniques is very complex and the results to date have been inconclusive.[29] As a result, the description of the fast intermolecular response of solvents reported in the literature, ranges from fully homogeneous to inhomogeneous. The most commonly used description fits the low frequency spectrum with a sum of antisymmetrized Gaussian and Ohmic functions.[13,30] The Gaussian-cage model is based on the premise that harmonic librational frequencies occur in a Gaussian (inhomogeneous) distribution of cages in the liquid.[31] The dynamics in the liquid is described by three parameters: the most probable frequency of oscillation, the spread in frequency, and the amplitude. The Ohmic distribution accounts for collision-induced dynamics.[32] More recently, the short-time-scale behavior of the liquid has been modeled by a small number of low frequency harmonic modes.[6,17] Although a sample consists of trillions of oscillators, experimental spectra can be fitted with only a small number of oscillators, suggesting that a few homogeneously broadened ''dominant modes'' drive the low frequency dynamics in the sample. Three parameters describe the liquid dynamics: the frequency of the mode, its damping rate, and its amplitude. Finally, the Kubo model[33] combines homogeneous and inhomogeneous contributions in a stochastic approach. Each mode requires four parameters: the modulation rate γ, the magnitude of the frequency fluctuation Δ, the center frequency, and an amplitude corresponding to the light scattering cross section of the respective intermolecular degree of freedom. In the extreme case when the value of the Kubo parameter $k = \Delta/\gamma$ is much larger than one, the line shape becomes Gaussian, reflecting an inhomogeneous distribution of frequencies. Conversely, in the case $k \ll 1$, the line shape becomes Lorentzian describing a fully homogeneous broadening. At intermediate values of k, the broadening is neither homogeneous nor inhomogeneous.

In practice, it is very difficult to distinguish between the various line-shape models by fitting the OHD-RIKES spectra. The large numbers of parameters, the lack of pronounced features in the spectra, and the resulting statistical correlation between parameters make an objective comparison of the relative quality of the fit difficult. Water, one of the most widely studied solvents, has been described variously (and successfully) with different functional forms including Lorentzian,[34] Gaussian,[35] Gaussian and Ohmic,[7] as well as more sophisticated models including both homogeneous and inhomogeneous broadening.[34,36] The molecules making up the ionic liquids studied here contain an imidazolium ring, which has a strong permanent dipole moment and is highly polarizable in the plane of the ring. Therefore, it is reasonable to assume that the imidazolium ring is responsible for the vast majority of the OHD-RIKES signal and that interaction-induced effects can be largely ignored. In addition, the ionic liquids studied here exhibit relatively sharp peaks in the low frequency spectra suggestive of motionally narrowed line shapes. Therefore, it is considered reasonable to assume in first instance that the intermolecular librational modes are homogeneously broadened. Any deviations, especially in the wings of the spectra, can then be attributed to a certain degree of inhomogeneous broadening including collisional broadening.[32] In practice, it is found that the homogeneous-broadening model provides a more intuitive picture of the liquid dynamics than a ''hybrid model'' including both homogeneous and inhomogeneous broadening. However, as in all previous OHD-RIKES studies, a good fit

of the theory to the data does not prove a particular broadening model.

The data from the OHD-RIKES experiments were analyzed in terms of the Brownian-oscillator model. This model has been described in detail in the literature[17] and only the strategic points will be discussed here. The nuclear motion is modeled by harmonic oscillators and each satisfies a generalized Langevin equation[17] whose response function in the frequency domain is given by

$$C(\omega)=(4/M)([\gamma-2i\omega]^2+4\Omega^2)^{-1}, \tag{3}$$

with $\Omega\equiv(\omega_0^2-\gamma^2/4)^{1/2}$ where γ denotes a damping rate, M the reduced mass, and ω_0 the undamped frequency of the mode under consideration. In the overdamped case, when the damping rate is significantly larger than the frequency of oscillation, the time-domain response function becomes

$$C(t)=\frac{H(t)}{M\gamma}[e^{-\omega_0^2 t/\gamma}-e^{-\gamma t}], \tag{4}$$

where $H(t)$ is the Heaviside step function. In the frequency domain this corresponds with

$$C(\omega)=\frac{1}{M\gamma}\left(\frac{\omega}{(\omega_0^2/\gamma)^2+\omega^2}-\frac{\omega}{\gamma^2+\omega^2}\right). \tag{5}$$

The first term in Eq. (4) corresponds to a decay with rate ω_0^2/γ, and the second term to a rise with rate γ. Therefore, the rate of decay of the underdamped Brownian oscillator corresponds with the rate of rise in the overdamped Brownian oscillator.

The experimental low-frequency spectra (up to 250 cm^{-1}) of the ionic liquids have been fitted to seven Brownian-oscillator functions as given by Eq. (3) (three for intermolecular librational modes, and four for intramolecular vibration) and one overdamped Lorentzian function as described by Eq. (5). The overdamped Lorentzian function accounts for rotational diffusion. The ''risetime frequency'' in Eq. (5) was chosen to be approximately equal to the first moment of the low-frequency spectral response of the sample. More specifically, this quantity was chosen to be equal to the damping rate of the three lowest frequency Brownian oscillators. This choice has been reported in previous studies[7] and is not entirely arbitrary as it represents a measurement of the reaction of the sample to a sudden impulse.

As the experimental spectra are fitted to such a large number of functions using such a large number of parameters, a proper analysis of the uncertainties in the parameters is essential. All data have been fitted using a nonlinear least-squares fitting program based on the simplex algorithm.[37] The resulting fit parameters are presented in Table I with uncertainties. The indicated uncertainties in the parameters are only due to ''lack of fit'' and ignore any systematic errors introduced by the subtraction of the diffusional response or uncertainty in the zero-delay position. The uncertainties in the fit parameters are 68.3% joint-confidence intervals[38] and therefore take into account uncertainties resulting from correlations between the parameters.

IV. GENERAL THEORY

Because the OHD-RIKES experiment employs very short pulses, a broad range of frequencies (several hundred cm^{-1}) will be excited. In molecular liquids, the sample polarizability will exhibit resonances, owing to rotational and vibrational motion. If these resonances arise from Raman-active modes, and they lie within the bandwidth of the laser, they may be coherently excited. Excitation of those modes contributes to the OKE signal, and the frequency of the mode can be detected in the time-resolved measurement. In this section, a classical expression of the OHD-RIKES signal will be derived.

The potential energy of a molecule in an external field can be expanded as a function of various orders of the field interacting with the dipole moment, polarizability, hyperpolarizability, etc., as $H=-\boldsymbol{\mu}_0\cdot\mathbf{E}-\frac{1}{2}\hat{\alpha}\cdot\mathbf{E}\cdot\mathbf{E}-\frac{1}{6}\hat{\beta}\cdot\mathbf{E}\cdot\mathbf{E}\cdot\mathbf{E}-\cdots$. The force exerted along the generalized coordinate ξ and defined as the first derivative of the potential energy with respect to that coordinate has therefore an infinite number of terms. The first two are relevant to our calculation, one being proportional to the permanent dipole moment $\boldsymbol{\mu}_0$, and the other proportional to the polarizability tensor $\hat{\alpha}$. If the potential energy of a molecule varies with the generalized coordinate ξ, its dipole moment and polarizability can be Taylor expanded with respect to that coordinate as

$$\begin{cases}\mu(\xi)=\mu_0+\mu'\xi+\cdots,\\ \alpha(\xi)=\alpha_0+\alpha'\xi+\cdots.\end{cases} \tag{6}$$

If it is assumed that a harmonic force drives the system back to equilibrium, the motion of the system is described by the Langevin equation,

$$\ddot{\xi}+\gamma\dot{\xi}+\omega_0^2(\xi_0+\xi)=M^{-1}(\boldsymbol{\mu}_0'\cdot\mathbf{E}+\tfrac{1}{2}\hat{\alpha}'\cdot\mathbf{E}\cdot\mathbf{E}+\cdots). \tag{7}$$

In this equation, M would correspond to the reduced mass if ξ refers to a vibrational coordinate x and M would correspond to the moment of inertia I if ξ refers to a librational (angular) coordinate θ. The first term on the right-hand side of Eq. (7) is responsible for IR absorption and the second one for Raman scattering.

The OHD-RIKES signal is proportional to the polarizability derivative with respect to a general coordinate (corresponding to vibrational or rotational motion) expressed in the laboratory frame.[17] This means that any motion affecting the ease of charge displacement of a molecule will be detected by Raman spectroscopy. Below, the motions that might occur in a liquid and their Raman activity will be reviewed. A (somewhat arbitrary) distinction must be made between the ''*intrinsic*'' polarizability and the polarizability that results from the presence of a *permanent dipole moment* in the molecule. The intrinsic polarizability is defined as a three-dimensional molecular property with often both isotropic and anisotropic components. The polarizability that results from the presence of a permanent dipole moment occurs because an external electric field can alter the projection of the dipole moment on the laboratory axes. Its value depends on the initial angle of the dipole moment of the molecule with respect to the polarization of the pump field.

TABLE I. Amplitude, frequency, and damping parameters of the six Brownian oscillators listed with their respective uncertainties for the five samples studied. The first (lowest frequency) Lorentzian corresponds to an overdamped Brownian oscillator. It is understood here that this component corresponds to a second rotational diffusion component with diffusion time shown in brackets. It is assumed that the three librational bands at approximately 30, 65, and 100 cm^{-1} correspond to three types of preferred location of the anion and that the relative amplitudes of these bands is equal to the probability of finding an anion in these locations. Adjacent to the amplitude parameters are listed the corresponding percentage amplitude of the three librational bands. The parameters listed for the last two oscillators at higher frequencies correspond to intramolecular vibrational modes.

Amplitude		ω (cm^{-1})	γ (cm^{-1})
		[bmim] [PF6]	
2±0.5		6±0.5(0.88 ps)	63
430±40	15%	32±1	63±5
780±60	27%	60±2	idem
1700±280	58%	90±3	idem
920±290		111±1	44±5
80±30		180±3	30±8
		[bmim] [Tf_2N]	
0.7±0.1		1.8±0.2(2.9 ps)	63
440±25	16%	29±0.1	63±3
730±40	26%	64±2	idem
1600±80	58%	100±2	idem
230±50		122±0.5	16±3
220±30		175±2	32±4
		[bmim] [TfO]	
0.8±0.1		3.4±0.2(1.56 ps)	64
400±20	14%	34±1	64±3
840±50	28%	70±1	idem
1700±200	58%	100±3	idem
200±200		120±2	35±10
120±60		173±2	30±6
		[bmmim] [Tf_2N]	
0.9±0.2		5±0.5(1.1 ps)	64
360±10	15%	30.6±0.5	64±1
510±10	22%	64±1	idem
1500±30	63%	100±1	idem
120±10		121.3±0.2	13±1
280±30		172±1	36±3
		[omim] [Tf_2N]	
0.33 ±0.05		1.8±0.2(2.9 ps)	81
500±50	18%	33±2	81±6
790±80	28%	69±3	idem
1500 ±150	54%	102±3 122±1	idem 14±2
120±20 240±160		174±2	35±10

A. Intramolecular vibration

Molecular vibrations *affect the localization of the charges within the molecule*. Both the isotropic and anisotropic part of the intrinsic molecular polarizability change with vibrational motion making intramolecular vibrations Raman active (apart from molecular-symmetry considerations).

B. Rotation and libration

The projection of the ''molecular polarizability'' component on the axis of the laboratory frame varies with rotation or libration of the molecule, which in turn leads to a Raman signal. As explained above the ''molecular polarizability'' arises from two components; the ''intrinsic'' polarizability and the polarizability that result from the presence of a permanent dipole moment. For both components of the ''molecular polarizability,'' rotation and libration are Raman active because they *affect the location of charges in space*.

C. Intermolecular vibration

An intermolecular vibration could be Raman active because (a) a polarizability change induced by one molecule on another through intermolecular vibration or (b) a system consisting of two oppositely charged molecules constitutes a polarizable unit. The relative position of a molecule with respect to another can affect the localization of charge on that molecule. However, this is a very weak effect and can be neglected in first approximation. In the case of a pair of oppositely charged molecules, it can be shown that the polarizability derivative with respect to an intermolecular vibrational coordinate is a function of the derivative of the amount of charge separation as

$$\frac{\partial \alpha}{\partial x} = C(\omega) \left. \frac{\partial q}{\partial x} \right|_{x_0}, \tag{8}$$

with $C(\omega)$ obtained by solving the Langevin equation Eq. (7). In the case of ions, the charge q is a constant leading to a polarizability change equal to zero, and no Raman activity.

D. Intermolecular libration

Similar to the case of a molecule librating, one can consider the dipole moment between anion and cation to librate and to be Raman active.

In conclusion, a Raman signal can have three sources: (1) intramolecular vibration changing the intrinsic polarizability, (2) rotation or libration altering the projection of an anisotropic intrinsic polarizability onto the laboratory axes, and (3) rotation or libration altering the projection of a permanent dipole moment onto the laboratory axes. It is not *a priori* obvious which of the latter two sources will be of greatest importance in determining the OHD-RIKES signal strength. In order to assess the relative strengths of these two sources, a theoretical librational model will be discussed.

A complete description of the signal due to libration would imply a derivation in three dimensions. However, a two-dimensional picture captures all the important physics and greatly simplifies the derivations. Figure 6 shows that both components of the signal (either due to the ''intrinsic'' polarizability or to the polarizability that result from the presence of a permanent dipole moment), are a function of a single coordinate θ. Depending on the nature of the polarizability, θ is either defined as the angle between the Z-axis of the molecule and the laboratory axis or, the dipole moment of the molecule (μ) and the laboratory axis. Therefore, Eq. (7) can be rewritten specifically for librational motion as

$$\ddot{\theta} + \gamma \dot{\theta} + \omega_0^2(\theta - \theta_0) = \frac{1}{I} F. \tag{9}$$

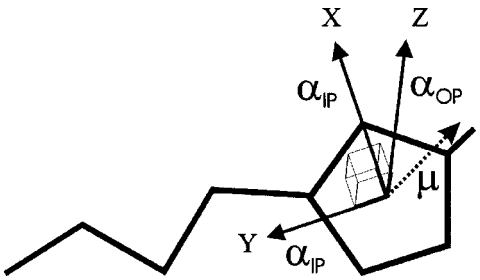

FIG. 6. In a two-dimensional picture of libration, changes of both ''intrinsic'' polarizability and polarizability resulting from the presence of a permanent dipole moment, are a function of a single coordinate θ. The components of the ''intrinsic'' polarizability in the plane of the imidazolium ring are considered to be equal and are denoted by α_{IP}. The component perpendicular to the ring along the *Z*-axis of the molecule is referred as α_{OP}. Depending on the nature of the polarizability, θ is either defined as the angle between the *Z*-axis of the molecule and the laboratory axis or between the dipole moment of the molecule (μ) and the laboratory axis.

It is reasonable to assume that the external perturbation from the pump pulse is weak making the deviation from equilibrium small. Considering an external electric field with components E_x and E_y in the laboratory frame, the potential of the dipole moment in the external field is $H=-\boldsymbol{\mu}(\theta)\cdot\mathbf{E}$ and the force can be calculated by taking the derivative with respect to angle θ. Using this expression for the force in Eq. (9), Fourier transformation can be used to solve the Langevin equation and it is found for $\tilde{\theta}(\omega)$ that

$$\tilde{\theta}=(\boldsymbol{\mu}'\cdot\mathbf{E}/I-\omega_0^2\theta_0)/((\omega-\omega_+)(\omega-\omega_-)), \tag{10}$$

with $\omega_\pm=-i\gamma/2\pm\Omega$, $\Omega\equiv\sqrt{\omega_0^2-\gamma^2/4}$. As the movement away from the equilibrium angle is perturbative, one can make a Taylor expansion of the dipole moment around the equilibrium and write an expression for the dipole moment in the presence of an external field in the frequency domain as $\boldsymbol{\mu}_{\text{total}}=\boldsymbol{\mu}_0+\boldsymbol{\mu}'\tilde{\theta}$, where $\boldsymbol{\mu}_0$ is the dipole moment vector (in the laboratory frame) without perturbation and $\boldsymbol{\mu}'\tilde{\theta}$ is the induced dipole moment vector. The molecular polarization is proportional to the induced dipole moment through the expression,

$$\mathbf{p}=\boldsymbol{\mu}'\tilde{\theta}=\boldsymbol{\mu}'\frac{\boldsymbol{\mu}'\cdot\mathbf{E}/I-\omega_0^2\theta_0}{(\omega-\omega_+)(\omega-\omega_-)}=\mathbf{p}_0+\hat{\alpha}\mathbf{E}. \tag{11}$$

This expression can be used to calculate the infrared absorption spectrum of the liquid.[6] Using Eq. (11) it is found that $\hat{\alpha}=\boldsymbol{\mu}'\otimes\boldsymbol{\mu}'/I(\omega-\omega_+)(\omega-\omega_-)$. In the case of Raman scattering, the frequency of the driving field tends to infinity. Therefore, one can make the approximation,

$$\hat{\alpha}_{\text{Raman}}\cong\frac{\boldsymbol{\mu}'\otimes\boldsymbol{\mu}'}{I\omega_{\text{laser}}^2}=\frac{\mu^2}{I\omega_{\text{laser}}^2}\begin{pmatrix}\sin^2\theta_0 & -\sin\theta_0\cos\theta_0\\ -\sin\theta_0\cos\theta_0 & \cos^2\theta_0\end{pmatrix}. \tag{12}$$

The effective dipole moment that allows interaction between the external (high frequency) field and the molecule is $\boldsymbol{\mu}_{\text{Raman}}=\hat{\alpha}_{\text{Raman}}\cdot\mathbf{E}_{\text{laser}}$. The macroscopic sample polarization produced through the Raman interaction can therefore be written as

$$\mathbf{P}_{\text{Raman}}=N\frac{\langle\alpha'_{\text{Raman},xx}\hat{\alpha}'_{\text{Raman}}\rangle E_{1x}^2}{(\omega-\omega_+)(\omega-\omega_-)I}\cdot\mathbf{E}_2\equiv\chi^{(3)}\mathbf{E}_1\cdot\mathbf{E}_1\cdot\mathbf{E}_2, \tag{13}$$

where N is the dipole-moment number density and the angled brackets stand for an orientational average.

In the slowly varying envelope approximation,[39] the amplitude of the probe field along the *z*-axis varies according to the linear differential equation $\partial\mathbf{E}_2/\partial z=\hat{\xi}\mathbf{E}_2$ with $\hat{\xi}=i\omega_L\chi^{(3)}E_1^2/2\varepsilon_0 c$. The solution is readily obtained and the retardation induced in the sample is expressed through the real and imaginary part of $\hat{\xi}$ by $\Gamma=\text{Im}(\xi_{XX})-\text{Im}(\xi_{YY})$. A Jones-matrix analysis (see Appendix) shows that the signal measured in our experimental setup is directly proportional to the retardation Γ. Equation (13) shows that $\xi_{XX}\propto\alpha'_{XX}\alpha'_{XX}$ and $\xi_{YY}\propto\alpha'_{XX}\alpha'_{YY}$. Therefore, the total heterodyne signal is proportional to $\langle(\hat{\alpha}'_{\text{Raman}})_{xx}(\hat{\alpha}'_{\text{Raman}})_{xx}-(\hat{\alpha}'_{\text{Raman}})_{xx}(\hat{\alpha}'_{\text{Raman}})_{yy}\rangle$ and the OKE signal (proportional to $\mathbf{E}\cdot\mathbf{P}_{\text{Raman}}$) is given by

$$S_{\text{OKE}}\propto\frac{N/I}{(\omega-\omega_+)(\omega-\omega_-)}\left(\frac{\mu^2}{I\omega_{\text{laser}}^2}\right)^2E^4. \tag{14}$$

In the same model, the intrinsic molecular polarizability $\hat{\alpha}_{\text{int}}$ can be written as a two-dimensional matrix with diagonal elements α_{IP} and α_{OP}. In transforming $\hat{\alpha}_{\text{int}}$ from the molecular to the laboratory frame, it can be expressed as the sum of an isotropic and anisotropic part as

$$(\hat{\alpha}_{\text{int}})_{\text{Lab}}=\begin{pmatrix}\alpha_{IP} & 0\\ 0 & \alpha_{IP}\end{pmatrix}+(\alpha_{OP}-\alpha_{IP})\times\begin{pmatrix}\sin^2\theta & -\sin\theta\cos\theta\\ -\sin\theta\cos\theta & \cos^2\theta\end{pmatrix}. \tag{15}$$

Comparing Eqs. (12) and (15) it can be noticed that the anisotropic component only differs in amplitude. Therefore the treatment of the signal will be identical to the case of the polarizability that result from the presence of a permanent dipole moment, and will be proportional to the square of the polarizability anisotropy following Eq. (14).

V. EXPERIMENTAL RESULTS AND DISCUSSION

Based on the theoretical analysis above, it can be concluded that the OHD-RIKES signal results from intermolecular librations and intramolecular vibrations. Libration describes the ''rocking'' of molecules in the field of neighboring molecules and raises the issue of the local structure. In this section, it will be shown how by fitting the spectra to a model using a number of Brownian oscillators, one can gain insight in the structure and dynamics of the ionic liquids studied.

The OHD-RIKES spectra of cyclohexane and DMSO (Fig. 2) have been described briefly in the Introduction. Now that the theory and the fitting procedure have been presented, one can explain the features in these spectra in more detail. For cyclohexane, a molecule with no permanent dipole mo-

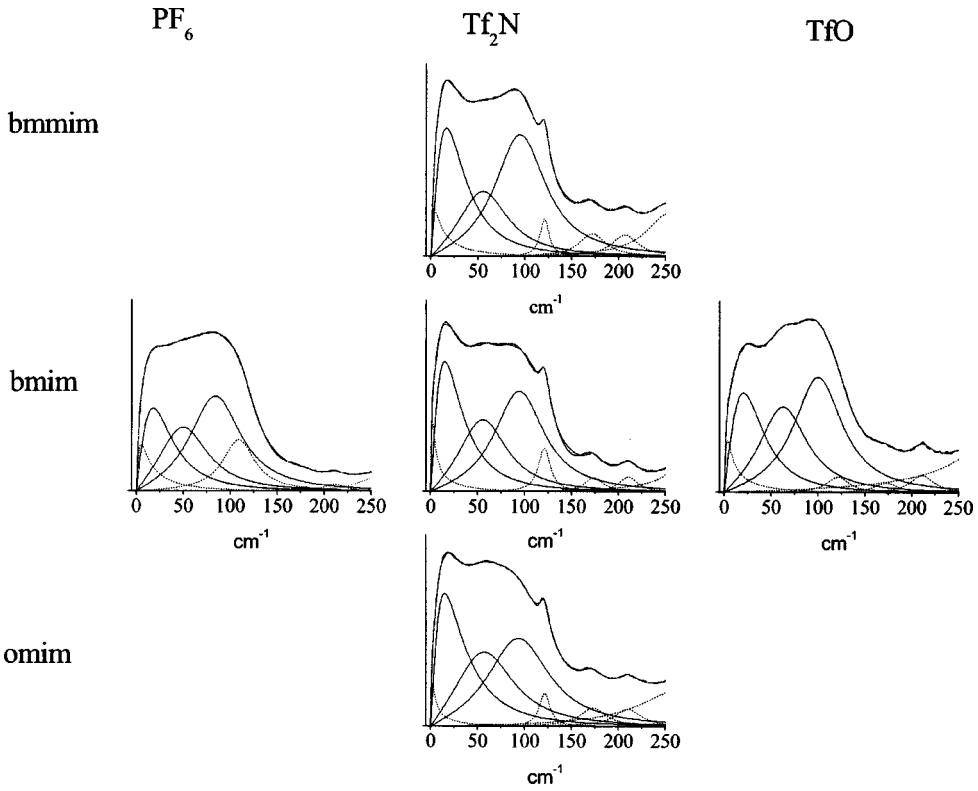

FIG. 7. OHD-RIKES spectra of ionic liquids classified according to their composition. The spectra have been fitted with the Brownian-oscillator model as described in the text. The dashed curve at very low frequency account for a residual rotational diffusion component in the sample, the solid lines represent librational motions, and the dashed lines at higher frequency represent intramolecular modes.

ment and very low polarizability, the signal must be due to the libration of an interaction-induced dipole moment. The weak intermolecular interactions in cyclohexane explain the relatively low frequency of the two Brownian oscillators at 25 and 53 cm^{-1}. DMSO has a permanent dipole moment and shows higher librational frequencies at 21, 54, and 91 cm^{-1}, consistent with the expected stronger intermolecular interactions. Figure 7 presents the spectra of five ionic liquids ordered according to their molecular composition. The vertical axis differentiates the cations and the horizontal axis the anions. The spectra have been fitted with the Brownian-oscillator model as explained above. Compared to polar organic solvents such as DMSO, the polarity of ionic liquids is the cause of even stronger intermolecular interactions and therefore of librations at higher frequencies. This is observed in the spectra of [bmim][Tf_2N] where the signal is fitted with three under-damped Brownian-oscillator functions at 15, 56, and 95 cm^{-1}. The large number of functions required to fit the spectra reflects the inhomogeneous nature of the sample on very short time scales.

Table I lists the fit parameters (amplitude, frequency, and damping rate) of the first six Lorentzian functions used to fit the experimental spectra and their respective uncertainties. The frequencies of the oscillators are well defined with errors of only $\approx$3% reflecting the sharp features in the experimental spectra of the ionic liquids. The damping and amplitude parameters are subject to uncertainties with an average error of $\sim$10%. This relatively large uncertainty is a result of the correlation between the amplitude and damping-rate parameters in the fit. The first (lowest frequency) Lorentzian corresponds to an overdamped Brownian oscillator. It is assumed here that this component corresponds either to a second rotational diffusion component (as the main rotational-diffusion component has been subtracted from the signal in the time domain) or to diffusive translational motions of the ''librational cage.'' [40] The diffusion time of this second component is shown in brackets. The next three low-frequency Lorentzian functions appear at roughly the same frequency in all ionic liquids studied and have similar fit parameters. Therefore, it is assumed that all three of these peaks correspond to libration of the imidazolium ring on the cation. In addition to these four relatively stable components in the spectra, a number of higher frequency peaks are seen that vary in frequency, width and amplitude in the various ionic liquids studied. It is assumed that these peaks correspond to intramolecular vibrational modes.

The five samples show three librational bands around 30, 65, and 100 cm^{-1}. Initially, the damping rates for these three bands were set as independent free parameters. During the fitting procedure, the damping-rate parameters of the first three nonoverdamped Brownian oscillators were found to be very close in all five samples. The damping rate is an indicator of how a particular motion couples to the bath. Therefore, similar damping between oscillators suggests that they undergo a similar type of motion, in our case a librational motion. From this point on, it was assumed that the damping rates of the three librational bands around 30, 65, and 100 cm^{-1} were in fact the same. In subsequent fitting of the data, the three damping parameters were linked resulting in a significant reduction of the calculated uncertainties in the remaining parameters.

As mentioned above, the diffusive part of the signal has been fitted to an exponential decay and subtracted in the time domain. To do so, the rate of rise of the diffusive response [denoted γ in Eq. (4)] had to be defined experimentally. In previous studies,[7] γ has been arbitrarily chosen to be the first

moment of the low frequency spectral density corresponding to an averaged intermolecular vibrational frequency. In our study, the damping rate of the first four oscillators was found to be approximately equal to the first moment of the spectrum. This suggests a kinetic picture in which the ''inertial state'' decays with a given rate into the ''diffusive state.'' This kinetic picture transforms the arbitrary assignment of the first moment of the spectrum to the rate of rise of the diffusional response into more legitimate choice.

In comparing the damping rates of the low-frequency Brownian oscillators between the different samples, it is seen that the magnitude is significantly higher for ionic liquids with a longer carbon chain, which are expected to interact more strongly with the bath. The sample $[\mathrm{omim}][\mathrm{Tf_2N}]$ has a damping-rate of 81 cm^{-1} compared to circa 64 cm^{-1} for the salts which only contain butyl substituents.

When comparing the relative amplitudes of the first three Brownian oscillators in the various spectra in Fig. 7, it appears that they depend on the nature of the anion. For the set of samples based on the $[\mathrm{Tf_2N}]$ anion the lowest frequency librational band (at $\sim$30 cm^{-1}) always shows the largest amplitude followed by the band at 100 cm^{-1}, followed by the band at 65 cm^{-1}. The set of samples based on a fixed cation does not show any pattern regarding the relative amplitudes of the three librational modes. The mode with the largest amplitude is that at 100 cm^{-1} for $[\mathrm{PF_6}]^-$ and $[\mathrm{TfO}]^-$ but that at 30 cm^{-1} for $[\mathrm{Tf_2N}]^-$. However, the parameters listed in Table I show that the amplitude of the third oscillator is greater than the second, which is in turn greater than the first oscillator for all five samples. The overdamped character of the first oscillator can explain this misleading observation. The changes in apparent amplitude are simply due to changes in damping rate and the fact that the oscillator at $\sim$30 cm^{-1} is close to being overdamped.

Neutron-scattering experiments[41] and computer simulations[42] have been conducted recently on 1,3-dimethylimidazolium chloride in the liquid phase. Both the experiment and the simulation results lead to the conclusion that there is a significant degree of order in the liquid salts for both long and short chain 1-alkyl-3-methylimidazolium salts. The picture that emerges is that each imidazolium is surrounded by three types of region of high probability for finding the anion. The largest probability density is on the CH bond on the symmetry axis (see Fig. 8), followed by a region on the other side of the molecule between the two CH groups and a pair of regions on either side of the ring. In contrast, the cation–cation correlation appears to be much weaker. Radial distributions have been computed for a number of room-temperature ionic liquids.[42–44] In the case of $[\mathrm{bmim}][\mathrm{PF_6}]$ (Ref. 44) it is found that the first three solvation shells for cation–anion pairs form at about 4.3, 10.6, and 17.6 Å, respectively. The long-range Coulombic interactions in the system allow a weak interaction to persist beyond 23 Å. Figure 8 shows a schematic probability distribution of the anion with respect to the cation according to calculations[42] on the chloride ion around dimethylimidazolium.

Thus, neutron-scattering experiments and computer simulations suggest that the anions can be found preferentially in three types of location with respect to the cation and

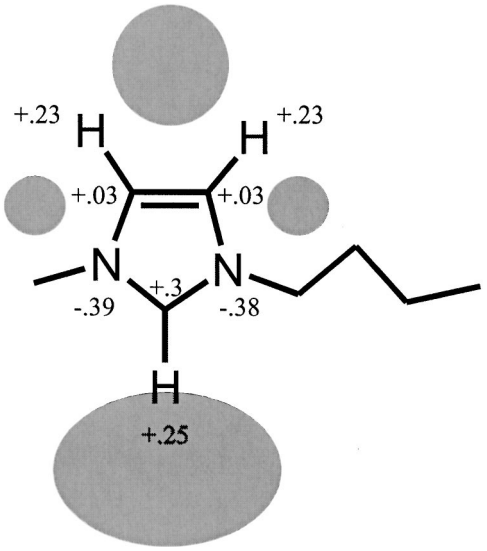

FIG. 8. Probability distribution of the counter ion around the 1-butyl-3-methylimidazolium cation based on computer simulations of a similar system (Ref. 42). The numbers represent calculated point charges at the atoms labeled.

our experiments show the presence of three librational bands at approximately 30, 65, and 100 cm^{-1}. This strongly suggests that the librational bands observed in the OKE spectra do in fact correspond with the three types of preferred location as shown in Fig. 8 and that the relative amplitudes of these bands is proportional to the probability of finding an anion in these locations. Following this logic, it can be deduced from Table I that the oscillators around 30, 65, and 100 cm^{-1} correspond respectively to 15%, 25%, and 60% of the anion population. Evaluation of the amplitude of the radial-distribution function for the chloride ion around dimethylimidazolium[42] reveals that the greatest anion density corresponds to 48% of the population followed by 35% and 17%. Those figures do not quite match our observation but show a similar trend. Based on this, it is tempting to conclude that 60% of the anions lie on the CH bond between the two nitrogen atoms of imidazolium ring, 25% are on the opposite side of the ring, and the remaining 15% are split on either side. Now that the frequencies have been assigned to molecular configurations, the next question is what kind of modes those frequencies correspond to.

To evaluate the different components of the librational response, one can draw conclusions based on the model described in the General theory, as well as from direct observation of the spectra and the fit parameters. The strength of the anisotropic molecular polarizability and induced polarizability component can be calculated from the model described in the previous section.

As discussed above, the signal due to the intrinsic anisotropic molecular polarizability is proportional to the square of the polarizability anisotropy. The aromatic imidazolium ring is the main source of polarizability anisotropy in the sample, orders of magnitude larger than the anion contribution. To our knowledge, the polarizability of the particular [bmim], [bmmim], and [omim] cations has not been reported. However the static polarizabilities of azole rings has

TABLE II. Dipole moment, effective dipole moment, and moment of inertia are listed for the three anions and the imidazolium ring. The polarizability derivative squared has been calculated and ordered by increasing value for the three components to the signal: (i) signal due to polarizability that result from the presence of a permanent dipole moment for the three anions, and the imidazolium ring, (ii) signal due to the libration of the dipole between an anion-and a cation for [bmim] [TfO], and (iii) signal coming from the polarizability anisotropy of the imidazolium ring.

	μ (D)	$\mu_{\text{effective}}$ (D)	$I\times10^{45}$ (kg m^2)	$(\alpha')^2\times10^{88}$ (F^2 m^4)
PF_6	0	0		0
Tf_2N	0.59	0.59	17	1.7×10^{-5}
bmim	5.9	1.8	1.3	0.25
TfO	4.4	4.4	3.78	1
[bmim] [TfO]				23
Polarizability anisotropy of the imidazolium ring				7.3×10^{8}

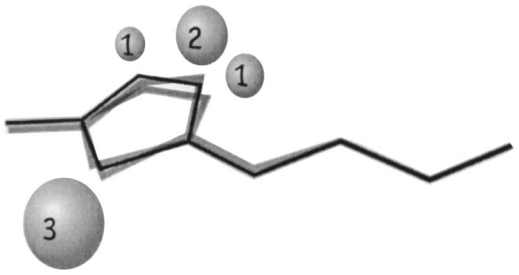

FIG. 9. Schematic of the out-of-plane librations of the imidazolium ring occurring in the three preferred positions of the anion (1), (2), and (3). In these positions of the anion the librational frequency is 30, 65, and 100 cm^{-1}, respectively, and the probability of finding the anion in these positions according to the analysis of the OHD-RIKES spectrum is 15%, 25%, and 60%, respectively.

been calculated and measured.[45] From a geometric point of view, the closest candidate to the cations used in our experiments is pyrrole. The values reported for pyrrole are 10.1×10^{-40} and 10.5×10^{-40} F m^2 for the components of the polarizability in the plane of the ring and 6.5×10^{-40} F m^2 for the component perpendicular to the ring. This implies that only out-of-plane motions will give rise to an OHD-RIKES or Raman-scattering signal. Out-of-plane librational motions can occur around two inertial axes, i.e., around the axis of the aliphatic chain and approximately perpendicular to it. Because these motions involve a similar moment of inertia and occur in a similar environment, they would appear at a similar frequency according to Eq. (14). Studies on benzene and substituted benzene corroborate this view. The OHD-RIKES spectra of substituted benzene[13,46] can be fitted to two modes around 20 and 70 cm^{-1} assigned to collision-induced and librational motion, respectively. Recent work on benzene[40] suggests that the low frequency mode (around 20 cm^{-1}) is caused by diffusive translational motions (vibration of the cage). Thus, the out-of-plane librational motions around the two inertial axes in the substituted benzenes are observed in the spectrum as a single ''mode.'' Considering that OHD-RIKES excites the sample relatively far from resonance, the static value of the polarizability is considered to be a good approximation. The signal was then calculated to be proportional to $S_{\text{PA}}\propto(\Delta\alpha)^2=7.29\times10^{-80}$ F^2 m^4.

The signal attributable to the polarizability that result from the presence of a permanent dipole moment is both a function of the magnitude of the permanent dipole moment and the moment of inertia of the molecule performing the librational motion [see Eq. (14)]. The charge distributions for [TfO], [Tf_2N], and [bmim] have been obtained from high-level density-functional theory. Table II lists the dipole moment, the effective dipole moment, the moment of inertia, and the predicted OHD-RIKES signal of the three anions and the imidazolium ring. The dipole moment and moment of inertia were calculated with respect to the center of mass of the molecule. For the cation, only librational motion of the imidazolium ring has been considered, and therefore only the dipole moment on the ring was taken into consideration. The effective dipole moment vector is defined as the component of the dipole vector perpendicular to the rotation axis. The imide ion [Tf_2N] has two different minimum energy geometries, with C_1 and C_2 symmetry, respectively.[47] Hartree–Fock calculations of the potential energy surface show that the C_2 configuration is the most stable with about 85% of the molecules in that state at room temperature. The values listed for Tf_2N in Table II have been calculated for the C_2 configuration. Finally, the signal coming from libration of the dipole moment between an anion and a cation has been calculated using

$$S_{\text{OHD-RIKES}}\propto\left(\frac{\mu^2}{I\omega_L^2}\right)^2=\left(\frac{4e^2}{\omega_L^2(m_A+m_C)}\right)^2 \tag{16}$$

with m_A and m_B the respective masses of the anion and cation.

Table II lists the predicted relative signal strength in the final column. The signal due to libration of the anion varies greatly with the value of the permanent dipole moment, from zero signal for [PF_6] to a maximum signal for [TfO] set as a reference. The signal strength of the cation ring due to the polarizability anisotropy is found to be 10^9 times larger than the signal that result from the presence of a permanent dipole moment. This shows that OHD-RIKES is blind to any dynamics of the anion. This is confirmed by the analysis of the spectra: The same number of Brownian oscillators can be used to represent the librational band of both [bmim][PF_6] and [bmim][TfO]. As the PF_6 ion has high symmetry, this shows that the anion does not influence the overall shape of the OHD-RIKES spectra and confirms that the signal is a measurement of the cation dynamics through the libration of its polarizability anisotropy.

Figure 9 is an attempt to represent the librational motion of the imidazolium ring in the three configurations previously described. For simplicity, only the libration around the hydrocarbon chain axis is represented. Libration will occur at defined frequencies corresponding to the relative position of the anion with respect to the cation. The signal amplitude is proportional to the average number of anions in a particular position. According to the amplitude fit parameters, 60% of the anion population lies on the CH bond between the two nitrogen atoms of imidazolium ring. This configuration gives rise to libration of the cation at about 100 cm^{-1}. Another 25% of the anion is positioned on the opposite side of the

ring leading to libration of the cation around 65 cm^{-1}. The remaining 15% is split on either side of the cation and is associated with libration of the ring at circa 30 cm^{-1}.

It is possible to draw some basic conclusions regarding the average time that an anion spends in any one of the three positions. The inhomogeneity in the sample is reflected by the three librational bands at 30, 65, and 100 cm^{-1} corresponding to a particular position of the anion with respect to the cation. The three peaks are separated by approximately 30 cm^{-1} and they are resolved in the spectrum rather than merged into a single peak. This indicates that if the anion can change its position relative to the cation, this must occur on a timescale longer than 1 ps. This number is consistent with recent simulations of the mean-square displacement of the ion as a function of time.[42,48] They show typically an initial rapid increase of the displacement attributed to rattling in the local cage and a slow asymptotic linear region corresponding to diffusion. In the case of [bmim][PF_6], the rapid increase stops at around 2 ps (Ref. 48) followed by a slow diffusion where the average ion moves only about 2 Å per ns,[44] showing that the lifetime of the ion in its environment is quite long. The damping rate γ corresponds to a dephasing rate and is proportional to the rate of cage fluctuation.

Finally, it should be acknowledged that the fits to the experimental spectra are not perfect suggesting a certain degree of inhomogeneity. In the two-body collision model introduced by Bucaro and Litovitz,[32] the shape of the spectrum is modified at high frequencies to a degree depending on the shape of the intermolecular interaction potential. This introduces a form of inhomogeneity to the spectra that is not included in our fit. Other forms of inhomogeneity, such as slow distortions of cage shape and concomitant spectral diffusion of the Brownian-oscillator frequencies, are also not included in our fitting model. In spite of this simplification, the fits are good, giving us full confidence in the method.

The minor variations in frequency of the librational modes described above is hard to explain with the crude description of our model. Previous studies reveal that both hydrogen bonded interaction and the interaction with the ring system may be present in the liquid and should therefore be considered in a more sophisticated model. Perhaps our experimental results will encourage a new theoretical analysis of the low frequency dynamics in ionic liquids.

Features at higher frequencies: In our OHD-RIKES setup, we can observe molecular frequencies as high as 600 cm^{-1} in the spectra with a good signal to noise ratio. Figure 10 shows the OHD-RIKES spectra in that window for the five samples studied. In the previous section it was shown that the low frequency part of the spectra (<200 cm^{-1}) is due to the librational and diffusive motions of the cation. In Fig. 10 it can be seen that there are Raman bands due to intramolecular vibrations in the anion, as well as the cation, over a very broad range of frequencies starting at a frequency as low as 120 cm^{-1}. Curves (b), (c), and (d) in Fig. 10 represent ionic liquids with the same anion $[Tf_2N]^-$ and present an identical feature at $\sim$300 cm^{-1} as well as a sharp peak at 120 cm^{-1} attributed to the anion CSN and CSO bending modes.[49] The $[TfO]^-$ anion [curve (e) in Fig. 10] shows two sharp lines at 300 cm^{-1} very distinct from those in (b), (c) and (d). Table III lists the observed vibrational frequencies for all five samples along with the calculated low frequency Raman band of the corresponding anion and their intensity. The calculations presented here have been obtained using GAUSSIAN 98, Revision A.9. It is not within the scope of this paper to consider the high frequency intramolecular vibrations in ionic liquid in detail and the assignment of the calculated vibrational frequencies presented here will be discussed elsewhere.

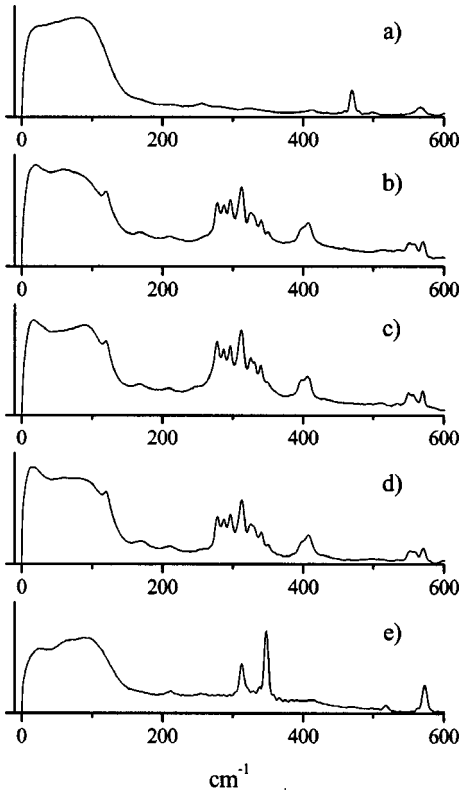

FIG. 10. OHD-RIKES spectra up to 600 cm^{-1} for (a) [bmim] [PF_6], (b) [omim] [Tf_2N]; (c) [bmmim] [Tf_2N]; (d) [bmim][Tf_2N]; (e) [bmim][TfO].

VI. CONCLUSION

Using the OHD-RIKES technique, we have measured the intermolecular dynamics of a series of five ionic liquids at room temperature: [bmmim][Tf_2N], [bmim][PF_6], [bmim][Tf_2N], [bmim][TfO], and [omim][Tf_2N]. Because of its relatively straightforward implementation and of its high signal to noise ratio, OHD-RIKES has been a widely applied method of capturing the ultrafast dynamics of a sample. Typical analysis involves conversion of time-domain data to a spectrum by deconvolution, followed by a fit of the spectrum using analytical line-shape functions. The latter may range from fully homogeneously broadened (such as the Brownian-oscillator model) to fully inhomogeneously broadened (Gaussian distributions) or models that can interpolate between the two (such as the Kubo line-shape theory). If the inhomogeneous broadening can be accessed using such analysis, its origin stays mostly unknown. Here the spectrum has been successfully fitted to a number of homogeneously broadened Brownian oscillators. As pointed out previously,[5] this may not give rise to the most perfect fit as a Gaussian

and a Lorentzian line shape have different ''tails.'' However, the tail region is where the systematic error in the experiment is largest since any time-delay error can masquerade as part of a line shape. In this paper, the Brownian-oscillator model has been proven to fit the OHD-RIKES spectra of organic and ionic liquids very well and to lead to a better understanding of the data.

All five samples have been fitted with three oscillators around 30, 65, and 100 cm^{-1} corresponding to out-of-plane libration of the cation imidazolium ring with the anion in three possible positions. Recent experimental and computer simulation studies on the structure of ionic liquids[41,42,44,48] shows that the relative position of the anion with respect to the cation is stable for a time on the order of 2 ps in the liquid phase and allowed us to assign those modes. According to the amplitude fit parameters, 60% of the anion population lies on the CH bond between the two nitrogen atoms of imidazolium ring. This configuration gives rise to libration of the cation at about 100 cm^{-1}. Another 25% of the anions is positioned on the opposite side of the ring leading to libration of the cation around 60 cm^{-1}. The remaining 15% is split on either side of the cation and are associated with libration of the ring at circa 30 cm^{-1}. Thus, the analysis of the spectrum in terms of Brownian oscillators has led to an improved understanding of the structure of the ionic liquids studied. The OHD-RIKES spectra of the various ionic liquids show more variation at frequencies above about 150–200 cm^{-1}, where the Raman bands of intramolecular modes are observed. The OHD-RIKES technique allows us to reach frequencies as high as 600 cm^{-1}.

OHD-RIKES is sensitive to the polarizability anisotropy. As such, it captures the dynamics of the cation because of its strong intrinsic polarizability, but is insensitive to any motion due to the anion. Infrared-absorption or terahertz[24] spectroscopy would be a complementary technique for its signal scales with the dipole moment of the molecule.[6] Another limitation of the OHD-RIKES technique is its incapability to distinguish between inhomogeneous and homogeneous contributions to the Raman line shape. Higher order Raman techniques could in principle make such as distinction (Table III).

TABLE III. Observed vibrational frequencies (cm^{-1}) of the five room-temperature ionic liquids studied along with the calculated Raman frequency and intensity of their respective anion.

Observed frequencies (cm^{-1})			Calculated Raman frequency (intensity)
[omim] $[Tf_2N]$	[bmmim] $[Tf_2N]$	[bmim] $[Tf_2N]$	$[Tf_2N]$ (C_2 rotamer)
119	119	119	106.7(1.14)
170	167	170	153.7(0.3533)
210	209	210	189.7(0.0509)
			195.7(0.1093)
	247	257	218.4(0.0287)
278	277	278	264.6(6.7742.)
287	286	287	277.6(3.213)
296	296	297	
			298.3(5.8024)
	[bmim][Pf_6]		[Pf_6]
	262		289.2 (0)
	[bmim][Tf]		[Tf]
	211		192.5(0.0547)
	256		296.9(4.3195)

ACKNOWLEDGMENTS

Financial support from EPSRC is gratefully acknowledged. In addition, acknowledgment is made to the donors of The Petroleum Research Fund, administered by the ACS for partial support of this research.

APPENDIX: BALANCED DETECTION

In the balanced-detection setup (Fig. 3), the probe beam is given either circular polarization with a quarter-wave retardation plate or 45° polarization with a half-wave retardation plate positioned after the sample. Horizontal and vertical components are separated with a Glan–Thompson polarizer and sent to a pair of photodiodes. The signals from the two photodiodes are subtracted electronically and sent to a lock-in amplifier. In this Appendix, it will be shown how the use of a quarter-wave retardation plate leads to a signal purely due to birefringence.

In order to derive the dependence of the signal on sample birefringence, it is necessary to work out the Jones matrix for both the retardation plate and the sample. In our OHD-RIKES setup, the pump beam is polarized at 45° with respect to the probe beam and the horizontal, resulting in a sample that acts like a retardation plate placed under an angle $\psi = 45°$. The Jones matrix of the sample is directly derived from the Jones matrix for a retardation plate with retardation Γ tilted under an angle ψ (Ref. 50) and is given by

$$W_{\text{sample}}(\Gamma) = \begin{pmatrix} \cos\frac{\Gamma}{2} & -i\sin\frac{\Gamma}{2} \\ -i\sin\frac{\Gamma}{2} & \cos\frac{\Gamma}{2} \end{pmatrix}. \tag{A1}$$

In order to give the probe beam circular polarization, a quarter-wave retardation plate ($\Gamma = 90°$) is placed under an angle of 45°, resulting in the Jones matrix,

$$W_{\text{wp}} = \begin{pmatrix} 1/\sqrt{2} & -i/\sqrt{2} \\ -i/\sqrt{2} & 1/\sqrt{2} \end{pmatrix}. \tag{A2}$$

Initially (before the sample, wave plate, and polarizer), the probe beam is horizontally polarized, which corresponds to the input Jones vector $(1,0)^T$. The output vector is given by the product of the input vector with the Jones matrices of the retardation plate and the sample as

$$W_{\text{wp}} W_{\text{sample}} \begin{pmatrix} 1 \\ 0 \end{pmatrix} = \begin{pmatrix} \cos\frac{\Gamma}{2} \Big/ \sqrt{2} - \sin\frac{\Gamma}{2} \Big/ \sqrt{2} \\ -i\cos\frac{\Gamma}{2} \Big/ \sqrt{2} - i\sin\frac{\Gamma}{2} \Big/ \sqrt{2} \end{pmatrix}. \tag{A3}$$

Finally, the photodiodes are wired up to subtract the horizontal from the vertical component of the probe beam intensity. Therefore, the strength of the signal sent to the lock-in amplifier is given by the difference of the horizontal with the vertical component of the output vector squared, i.e.,

$$I_h - I_v = -\sin\Gamma. \tag{A4}$$

This shows that if the retardation induced by the pump is small (which is the case in the experiment), the signal is linearly proportional to the birefringence phase angle Γ in the sample. Following the same reasoning, it can be shown that the use of a half-wave retardation plate after the sample results in a signal purely due to dichroism.

[1] K. R. Seddon, J. Chem. Technol. Biotechnol. **68**, 351 (1997); C. M. Gordon, Appl. Catal., A **222**, 101 (2001); R. Sheldon, Chem. Commun. (Cambridge) **23**, 2399 (2001); P. Wasserscheid and W. Keim, Angew. Chem., Int. Ed. Engl. **39**, 3772 (2000); T. Welton, Chem. Rev. **99**, 2071 (1999); J. D. Holbrey and K. R. Seddon, in *Clean Products and Processes*, edited by T. Matsunaga (Springer-Verlag, Berlin, 1999), Vol. 1, pp. 223–236.

[2] G. A. Voth and R. M. Hochstrasser, J. Phys. Chem. **100**, 13034 (1996).

[3] M. C. Beard, G. M. Turner, and C. A. Schmuttenmaer, J. Phys. Chem. B **106**, 7146 (2002).

[4] R. Huber, A. Brodschelm, F. Tauser, and A. Leitenstorfer, Appl. Phys. Lett. **76**, 3191 (2000).

[5] N. A. Smith and S. R. Meech, Int. J. Radiat. Phys. Chem. **21**, 75 (2002).

[6] G. Giraud and K. Wynne (unpublished).

[7] Y. Chang and E. W. Castner, J. Chem. Phys. **99**, 7289 (1993).

[8] E. W. Castner, Y. J. Chang, J. S. Melinger, and D. McMorrow, J. Lumin. **60&61**, 723 (1994).

[9] A. Idrissi, P. Bartolini, M. Ricci, and R. Righini, J. Chem. Phys. **114**, 6774 (2001).

[10] G. Giraud and K. Wynne, J. Am. Chem. Soc. **124**, 12110 (2002).

[11] M. L. T. Asaki, A. Redondo, T. A. Zawodzinski, and A. J. Taylor, J. Chem. Phys. **116**, 10377 (2002).

[12] H. Weingartner, A. Knocks, W. Schrader, and U. Kaatze, J. Phys. Chem. A **105**, 8646 (2001).

[13] Y. J. Chang and E. W. Castner, J. Phys. Chem. **100**, 3330 (1996).

[14] G. P. Johari, J. Non-Cryst. Solids **307–310**, 114 (2002).

[15] The following abbreviations are used when referring to the ionic liquids: $[\mathrm{bmim}]^+ = 1\text{-butyl-}3\text{-methylimidazolium}$, $[\mathrm{bmmim}]+ = 1\text{-butyl-}2,3\text{-dimethylimidazolium}$, $[\mathrm{omim}]^+ = 1\text{-methyl-}3\text{-octylimidazolium}$, $[\mathrm{TfO}]^- = \mathrm{CF3SO3}\text{-(trifluoromethanesulfate or triflate anion)}$, *and* $[\mathrm{Tf2N}]^- = (\mathrm{CF3SO2})2N\text{-}(bis(\text{trifluoromethanesulfonyl})\text{imide})$.

[16] P. Bonhote, A. P. Dias, N. Papageorgiou, K. Kalyanasundaram, and M. Gratzel, Inorg. Chem. **35**, 1168 (1996).

[17] M. Cho, M. Du, N. F. Scherer, G. R. Fleming, and S. Mukamel, J. Chem. Phys. **99**, 2410 (1993).

[18] N. A. Smith, S. J. Lin, S. R. Meech, H. Shirota, and K. Yoshihara, J. Phys. Chem. A **101**, 9578 (1997).

[19] J. G. Huddleston, H. D. Willauer, R. P. Swatloski, A. E. Visser, and R. D. Rogers, Chem. Commun. (Cambridge) **1998**, 1765.

[20] K. R. Seddon, A. Stark, and M. J. Torres, Pure Appl. Chem. **72**, 2275 (2000).

[21] M. T. Asaki, C.-P. Huang, D. Garvey, J. Zhou, H. C. Kapteyn, and M. M. Murnane, Opt. Lett. **18**, 977 (1993).

[22] D. T. Reid, W. Sibbett, J. M. Dudley, L. P. Barry, B. Thomsen, and J. D. Harvey, Appl. Opt. **37**, 8142 (1998).

[23] D. McMorrow, W. T. Lotshaw, and G. A. Kenney-Wallace, IEEE J. Quantum Electron. **24**, 443 (1988).

[24] K. Wynne, J. J. Carey, J. Zawadzka, and D. A. Jaroszynski, Opt. Commun. **176**, 429 (2000).

[25] D. McMorrow and W. T. Lotshaw, Chem. Phys. Lett. **174**, 85 (1990).

[26] D. McMorrow, Opt. Commun. **86**, 236 (1991).

[27] T. Steffen and K. Duppen, J. Chem. Phys. **106**, 3854 (1997).

[28] K. Okumura, A. Tokmakoff, and Y. Tanimura, Chem. Phys. Lett. **314**, 488 (1999).

[29] K. J. Kubarych, C. J. Milne, S. Lin, V. Astinov, and R. J. D. Miller, J. Chem. Phys. **116**, 2016 (2002).

[30] Y. J. Chang and E. W. Castner, J. Phys. Chem. **98**, 9712 (1994); D. McMorrow, N. Thantu, J. S. Melinger, S. K. Kim, and W. T. Lotshaw, *ibid.* **100**, 10389 (1996).

[31] R. M. Lynden-Bell and W. A. Steele, J. Phys. Chem. **88**, 6514 (1984).

[32] J. A. Bucaro and T. A. Litovitz, J. Chem. Phys. **54**, 3846 (1971).

[33] R. Kubo, Adv. Chem. Phys. **15**, 101 (1969); K. A. Wood and H. L. Strauss, J. Phys. Chem. **94**, 5677 (1990).

[34] Y. Tominaga, Y. Wang, A. Fujiwara, and K. Mizoguchi, J. Mol. Liq. **65-6**, 187 (1995).

[35] G. E. Walrafen, J. Phys. Chem. **94**, 2237 (1990).

[36] K. Winkler, J. Lindner, and P. Vohringer, Phys. Chem. Chem. Phys. **4**, 2144 (2002).

[37] W. H. Press, S. A. Teukolsky, W. T. Vetterling, and B. P. Flannery, *Numerical Recipes in C* (Cambridge University Press, Cambridge, 1992).

[38] G. A. Seber and C. J. Wild, *Nonlinear Regression* (Wiley, New York, 1989).

[39] Y. R. Shen, *The Principles of Nonlinear Optics* (Wiley, New York, 1984).

[40] M. Ricci, P. Bartolini, R. Chelli, G. Cardini, S. Califano, and R. Righini, Phys. Chem. Chem. Phys. **3**, 2795 (2001); R. Chelli, G. Cardini, M. Ricci, P. Bartolini, R. Righini, and S. Califano, *ibid.* **3**, 2803 (2001); B. Ratajska-Gadomska, J. Chem. Phys. **116**, 4563 (2002).

[41] C. Hardacre, J. D. Holbrey, S. E. J. McMath, D. T. Bowron, and A. K. Soper, J. Chem. Phys. **118**, 273 (2003).

[42] C. G. Hanke, S. L. Price, and R. M. Lynden-Bell, Mol. Phys. **99**, 801 (2001).

[43] J. de Andrade, E. S. Boes, and H. Stassen, J. Phys. Chem. B **106**, 13344 (2002).

[44] T. I. Morrow and E. J. Maginn, J. Phys. Chem. B **106**, 12807 (2002).

[45] K. E. Calderbank, R. L. Calvert, P. B. Lukins, and G. L. D. Ritchie, Aust. J. Chem. **34**, 1835 (1981); N. E. B. Kassimi, R. J. Doerksen, and A. J. Thakkar, J. Phys. Chem. **99**, 12790 (1995).

[46] N. A. Smith and S. R. Meech, J. Phys. Chem. A **104**, 4223 (2000).

[47] P. Johansson, S. P. Gejji, J. Tegenfeldt, and J. Lindgren, Electrochim. Acta **43**, 1375 (1998).

[48] C. J. Margulis, H. A. Stern, and B. J. Berne, J. Phys. Chem. B **106**, 12017 (2002).

[49] I. Rey, P. Johansson, J. Lindgren, J. C. Lassegues, J. Grondin, and L. Servant, J. Phys. Chem. A **102**, 3249 (1998).

[50] A. Yariv, *Optical Electronics Communications*, 5th ed. (Oxford University Press, Oxford, 1997).